Modelling of heat and mass transfer from spheroidal drops with general non-uniform Dirichlet boundary conditions

G. Varma Raja Kochanattu*, G.E. Cossali, S. Tonini
Department of Engineering and Applied Sciences, University of Bergamo, Italy
*Corresponding author: g.varmarajakochan@studenti.unibg.it

INTRODUCTION

The process of liquid drop evaporation has wide range of applicative fields like spray combustion, spray painting, fire control, medical applications, etc. [1]. The modelling of evaporation of liquid droplets in gaseous environment has been extensively studied since Maxwell proposed the first model [2]. The classical approach for modelling this problem includes some assumptions like drop sphericity, constant gas density and properties, ignoring the Dufour and Soret effects, etc. 1-D analytical approach for modelling evaporation of deformed droplet was developed in [3]. The effect of non-uniform drop surface temperature on the heating and evaporation of spheroidal droplet was initially studied in [4], which proposes an analytical solution for the steady-state species conservation equations and a numerical solution for the energy equation for spheroidal drops in gaseous mixture, imposing non-uniform drop temperature profiles. The results suggested that the correlation of the vapor flux as function of the Gaussian curvature [3] holds only with uniform drop temperature case. The application of the model to the study of the transient drop heating and evaporation was first proposed in [5], enlightening the contribution of drop temperature non-uniformity on heat and mass transport within the liquid phase. The present work extends the model to general non-uniform Dirichlet boundary conditions, including the variation of the drop temperature along the azimuthal angle, proposing a fully 3-D analytical solution of the species conservation equation for spheroidal drops. The next sections describe the mathematical modelling and the analytical solution proposed, followed by same samples of the results obtained applying the model to spherical and spheroidal geometries under different operating conditions. Extension to the solution of the energy equation will be part of a future work.

MATHEMATICAL MODELLING

CONSERVATION EQUATIONS

The steady-state species conservation equations can be written in the general form for a binary system as:

$$\nabla_j n_j^{(\alpha)} = 0 \tag{1}$$

where the mass flux $n_j^{(\alpha)}$ (with α = (1, 2) for gas and vapour, respectively) assumes the form:

$$n_j^{(\alpha)} = \rho U_j \chi^{(\alpha)} - \rho D_v \chi^{(\alpha)} \tag{2}$$

where $\chi^{(\alpha)} = \frac{\rho^{(\alpha)}}{\rho}$ is the mass fraction, D_v is the mass diffusivity and U_j is the Stefan flow velocity. Using equations (1) and (2) and accounting for $\chi^{(1)} + \chi^{(2)} = 1$ yields the usual mass conservation equation $\nabla_j \left(\rho U_j\right) = 0$. Assuming still drop surface and neglecting gas diffusion within the liquid phase yields nil gas flux everywhere. Defining $G = \ln\left(1 - \chi^{(2)}\right)$, the equation (2) becomes:

$$U_j = D_v \nabla_j G \tag{3}$$

and under further assumption of constant diffusion coefficient, the Laplace equation for the variable G is obtained:

$$\nabla^2 G = 0 \tag{4}$$

The steady-state energy equation, neglecting minor terms like dissipation by viscous stress, and assuming constant transport properties within the gas mixture (refer to [6] for the complete expression), can be written as:

$$U_j \nabla_j T = \frac{k}{\rho c_p} \nabla^2 T \tag{5}$$

Using equation (3), equation (5) becomes:

$$\frac{\rho c_p D_v}{k} \nabla_j G \nabla_j T - \nabla^2 T = 0 \tag{6}$$

The present model proposes an analytical solution of equation (4) for spherical and spheroidal drops, imposing non-uniform Dirichlet boundary conditions at the drop surface.

SOLUTION IN SPHERICAL AND SPHEROIDAL COORDINATE SYSTEMS

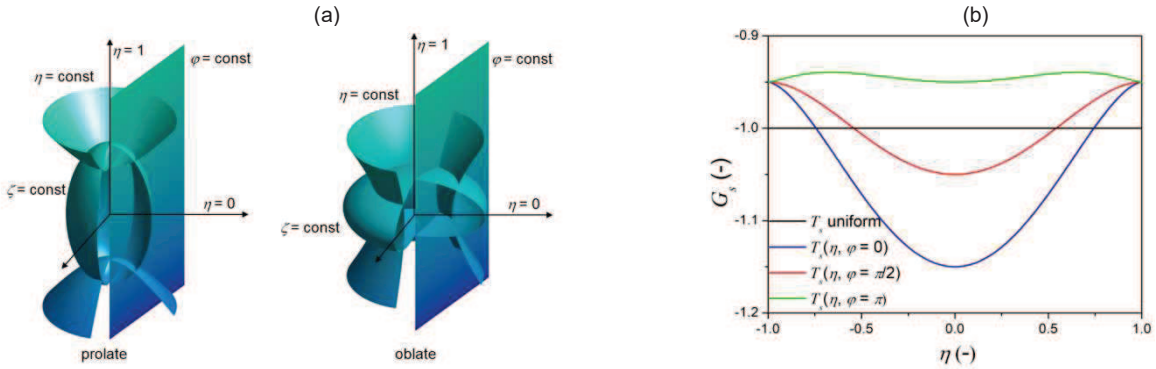

Figure 1: (a) Spheroidal coordinate system configuration: oblate (left), prolate (right). (b) η-profiles of the variable G at the drop surface for the different test-cases investigated.

The Laplace equation (4) was solved in spherical and spheroidal oblate and prolate coordinate systems, which definitions are given by the equations (7) (refer to figure 1a for a schematic configuration) [7]:

$$x = a\sqrt{\zeta^2+\alpha}\sqrt{1-\eta^2}\cos\phi;\;\; y = a\sqrt{\zeta^2+\alpha}\sqrt{1-\eta^2}\sin\phi;\;\; z = a\zeta\eta \tag{7}$$

where α is equal to 0, -1, +1 for the spherical, prolate spheroidal and oblate spheroidal geometries, respectively. The drop surface is always defined by the equation $\zeta = \zeta_0$, although it must be noticed that the coordinates η and ζ have different definitions in the different coordinate systems, as an example, $\zeta = R_0/r$ and $\eta = \cos\theta$ for the spherical coordinates, where R_0 is the radius of the spherical particle defined by the equation $\zeta = 1$ (i.e. $\zeta_0 = 1$). To notice that for a general shaped drop, an equivalent radius can be always defined as: $R_0 = \sqrt[3]{3V/4\pi}$, where V is the drop volume. In the following, the drop size will be always defined to maintain the same equivalent radius allowing a direct comparison of the evaporation characteristics of different shaped drops having the same volume.

The scale parameter in equations (7) is defined as $a = R_0\dfrac{\left|1-\varepsilon^2\right|^{1/2}}{\varepsilon^{1/3}}$, where $\varepsilon = \dfrac{a_z}{a_r}$ is the deformation parameter defined with respect to the axial (a_z) and radial (a_r) semi-axis. The analytical solution for the Laplace equation (4) assumes the following form [7]:

$$G - G_\infty = \sum_{n,m} g_{n,m} W_n(\zeta) P_n^m(\eta)\cos(m\varphi) \tag{8}$$

where $P_n^m(\eta)$ are the associated Legendre functions of the first kind [8] and the functions $W_n(\zeta)$ depend on the coordinate system:

$$W_n(\zeta) = \frac{\zeta^{n+1}(\zeta)}{\zeta_0^{n+1}(\zeta_0)}\;\; sphere;\;\; W_n(\zeta) = \frac{Q_n^m(\zeta)}{Q_n^m(\zeta_0)}\;\; prolate;\;\; W_n(\zeta) = \frac{Q_n^m(i\zeta)}{Q_n^m(i\zeta_0)}\;\; oblate \tag{9}$$

where Q_n^m are the associated Legendre functions of the second kind [8].

The coefficients g_{nm} are calculated imposing the boundary conditions at the drop surface. The values of the drop temperature on the drop surface are imposed and the corresponding values of the variable G are calculated assuming that the vapour is saturated in the region close to the liquid/drop interface. To notice that the function G on the surface is monotonically decreasing with surface temperature. The selected profile of the temperature and the function G at the drop surface should satisfy some constrains: the symmetry conditions at the pole $\eta = 1$ yields $\partial G/\partial\eta = 0$; the symmetry at the equator yields $G_s(\eta,\varphi) = G_s(-\eta,\varphi)$. Furthermore the knowledge of the minimum and maximum values of the temperature profile, and then of the function G on the surface, assumed monotonic along the variable η, assures the closure of the problem. Figure 1(b) shows a sample of the distribution of G as function of the coordinate η along the drop surface, for three values of the azimuthal angle φ.

Once the solution of the species conservation equation is obtained, the vapour fluxes can be calculated along each coordinate directions:

$$n_{v,j} = \rho D_v \nabla_j G \quad with\; j = (\zeta,\eta,\varphi) \tag{12}$$

where the gradients of the variable G assume the form:

$$\nabla_\zeta G = \frac{1}{h_\zeta}\sum_{n,m} g_{n,m} W_n'(\zeta) P_n^m(\eta)\cos(m\varphi) \tag{13a}$$

$$\nabla_\eta G = \frac{1}{h_\eta}\sum_{n,m} g_{n,m} W_n(\zeta) P_n^{m'}(\eta)\cos(m\varphi) \tag{13b}$$

$$\nabla_\varphi G = -\frac{1}{h_\varphi}\sum_{n,m} m g_{n,m} W_n(\zeta) P_n^m(\eta)\sin(m\varphi) \tag{13c}$$

being $W_n^{'}$ the derivatives with respect to ζ *and* $P_n^{m'}$ the derivative with respect to η.

RESULTS AND DISCUSSION

The model has been applied to calculate the effect of different boundary conditions at the drop surface on the vapour flux distribution for spherical and spheroidal drops. Three different boundary conditions have been investigated, namely a uniform distribution of the surface temperature, a distribution only function of the variable η and a distribution function both of the variable η and the azimuthal angle φ. The three distributions have been applied to three drop shapes having the same volume: a spherical drop, a spheroidal prolate drop with ε = 1.5 and a spheroidal oblate drop with ε = 0.5. Figure 1(b) shows the corresponding profiles of the variable $G = \ln\left(1-\chi^{(2)}\right)$, along the drop surface as function of the η-coordinate. The test-case with temperature and G only function of the variable η corresponds to the profile with $G_s(\eta, \varphi = \pi/2)$, while for the test case with the temperature and G function of both coordinates η and φ, three profiles have been plotted as a sample, corresponding to φ=0, π/2 and π. Figure 2 shows the contour distribution of the ζ-component of the non-dimensional vapour flux defined as $\tilde{n}_{v,\zeta} = \dfrac{n_{v,\zeta} R_0}{\rho D_v (G_\infty - G_s)}$ at the drop surface imposing uniform drop temperature for the two spheroidal drops, while the arrows represent the flux vectors. The graphs shows that the flux is depending on the drop curvature, and for the particular case with uniform temperature conditions at the drop surface the flux results to be proportional to the fourth root of the drop Gaussian curvature, as found in [3]. This is confirmed in figure 3(a), which plots the profile along the η-coordinate of the non-dimensional flux for the spherical and two spheroidal drop shapes imposing the uniform temperature distribution at the drop surface. The corresponding profiles obtained imposing a temperature distribution only function of the η-coordinate (red profile of figure 1b) are reported in figure 3(b). The imposed temperature has a peak at the drop equator (minimum of G_s) and a minimum at the poles (maximum of G_s). The vapour flux for the oblate drop reflects the imposed boundary conditions, with the maximum value reached at the drop equator and minimum values at the drop poles. For spherical and prolate drops the minimum value of the non-dimensional vapour flux is not reached at the poles and this is more evident in the case of prolate drop where the curvature is higher at the drop poles.

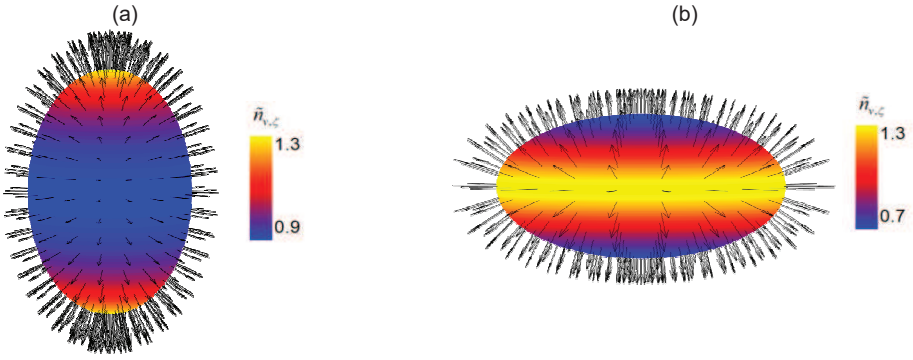

Figure 2: Non-dimensional vapour flux distribution at the drop surface for (a) prolate (ε = 1.5) and (b) oblate (ε = 0.5) drop with uniform temperature distribution as boundary conditions.

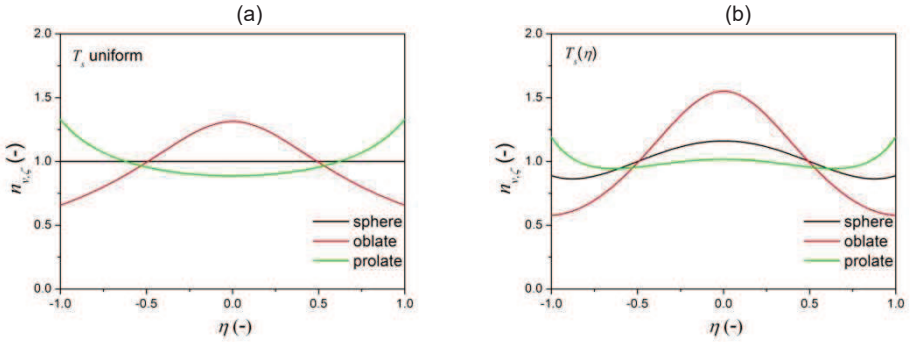

Figure 3: Non-dimensional vapour flux profiles along η-coordinate for spherical, prolate (ε = 1.5) and oblate (ε = 0.5) drops with (a) uniform temperature distribution and (b) temperature distribution function of η.

The effect of more general temperature distribution on the non-dimensional vapour flux distribution is shown in figure 4 for the three drop shapes. The corresponding profiles of the variable G_s as function of the h-coordinate along three azymuthal angles are reported in figure 1(b). The results suggest that the complexity of the temperature distribution reflects to the disuniformity of the vapour fluxes, and this is particularly evident for the

oblate drop, as confirmed by the distribution of the non-dimensional vapour flux as function of η-coordinate reported in figure 5 for all the three selected drop shapes.
This evidences the importance of accounting for non-uniform temperature distribution when modeling deformed drop evaporating in stagnant air. The model may be extended to include the solution of the energy equation to predict the combined effect of heat and mass transport within the gas mixture for spherical and spheroidal drops with non-uniform boundary conditions at the drop surface. This represents the main target for future investigation.

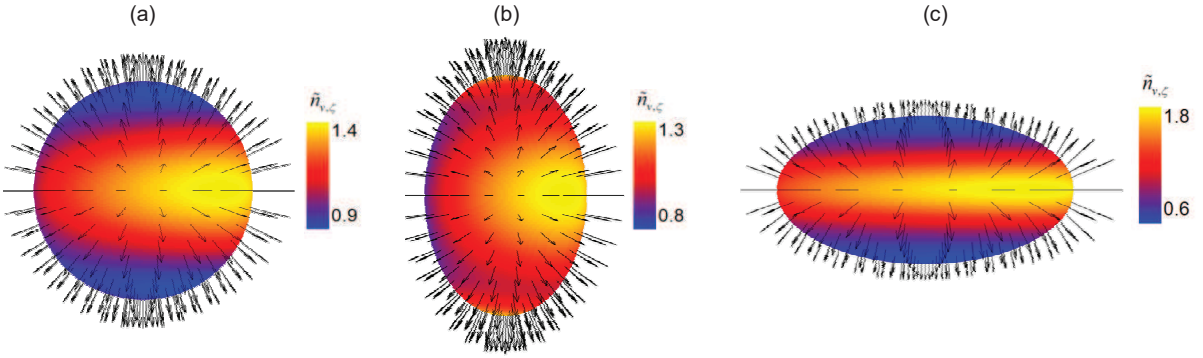

Figure 4: Non-dimensional vapour flux distribution at the drop surface for (a) sphere, (b) prolate (ε = 1.5) and (c) oblate (ε = 0.5) drop with non-uniform temperature distribution as boundary conditions.

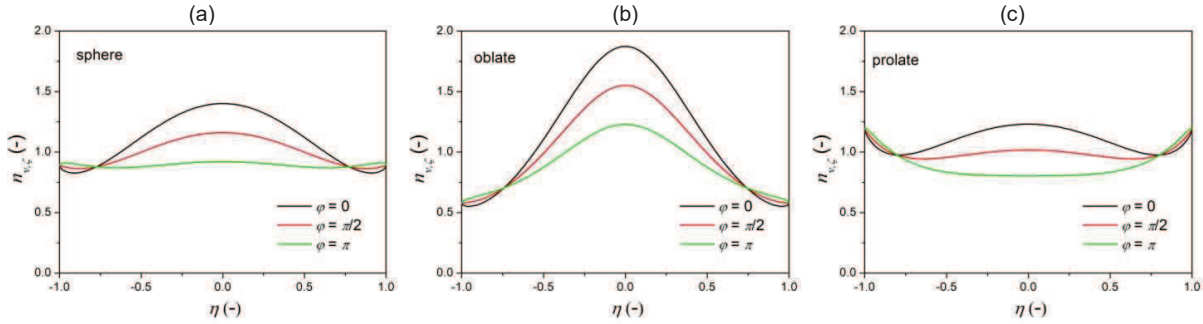

Figure 5: Non-dimensional vapour flux profiles along η-coordinate for three azymuthal angles φ, for (a) sphere, (b) prolate (ε = 1.5) and (c) oblate (ε = 0.5) drops with non-uniform temperature distribution as boundary conditions.

CONCLUSION AND NEXT STEP IN RESEARCH

The steady-state analytical solution of the species conservation equations has been analysed for spherical and spheroidal drops evaporating in stagnant air by accounting for the effect of non-uniform drop temperature as boundary conditions at the liquid/drop interface. The model has been applied to predict the vapour flux distribution for three drop shapes imposing different temperature distribution at the drop surface. The model will be extended to include the solution of the energy equation accounting for the combined effect of heat and mass transfer on a drop evaporating in a gas mixture.

References

[1] Crowe, C.T., Sommerfeld, M., Tsuji, Y., Multiphase Flows with Droplets and Particles, CRC Press, 1998.
[2] Maxwell, J.C., 9th edition, Diffusion, Encyclopaedia Britannica, 1877.
[3] Tonini, S., Cossali, G.E., International Journal of Heat and Mass Transfer 97: 301-7 (2016).
[4] Tonini, S., Cossali, G.E., International Journal of Heat and Mass Transfer 121: 747–758 (2018).
[5] Zubkov, V.S., Cossali, G.E., Tonini, S., Rybdylova, O., Crua, C., Heikal, M., Sazhin, S.S., International Journal of Heat and Mass Transfer 108: 2181–2190 (2017).
[6] Slattery, J.C., Momentum, Energy and Mass Transfer in Continua, 2nd-edition, R. Krieger Publ. New York, 1981.
[7] Moon, P., Spencer, D.E., Field theory handbook: Including Coordinate Systems, Differential Equations and their Solutions, Springer, 2012.
[8] Olver, F.W.J., Lozier, D.W.R., Boisvert, F., Clark, C.W., NIST handbook of Mathematical functions, 2010.